

Terahertz evidence of electromagnon excitations in the multiferroic van der Waals insulator NiI₂Jae Ha Kim ¹, Taek Sun Jung ¹, Youjin Lee,² Chaebin Kim ², Je-Geun Park ^{2,*} and Jae Hoon Kim^{1,†}¹*Department of Physics, Yonsei University, Seoul 03722, Republic of Korea*²*Center for Quantum Materials and Department of Physics and Astronomy, Seoul National University, Seoul 08826, Republic of Korea*

(Received 6 April 2023; accepted 27 July 2023; published 10 August 2023)

We report on our terahertz spectroscopic investigation of the van der Waals insulator NiI₂, exhibiting antiferromagnetism below $T_{N1} \simeq 78$ K and multiferroicity below $T_{N2} \simeq 59.5$ K. Two electromagnon modes were detected at 34 and 37 cm⁻¹ below T_{N2} where the material is in the helimagnetic-multiferroic phase. Our transmission measurement shows that the electromagnon resonance modes redshift with increasing temperature (at zero magnetic field) but blueshift with increasing magnetic field (at 1.5 K). A separate reflection measurement confirms the electric dipole active nature of the two electromagnon modes. The polarization, temperature, and magnetic field dependences show that these electromagnon modes are closely linked with the helimagnetic ordering in the multiferroic phase of NiI₂. The electromagnon energies are also consistent with the energy scale of the two-magnon sideband excitation around the Zhang-Rice exciton mode recently discovered in NiI₂.

DOI: [10.1103/PhysRevB.108.064414](https://doi.org/10.1103/PhysRevB.108.064414)**I. INTRODUCTION**

NiI₂ is a layered quasi-two-dimensional van der Waals insulator. The individual layer consists of corner-sharing NiI₆ octahedra, while Ni atoms themselves constitute a triangular lattice [Fig. 1(a)]. The superexchange magnetic interaction between NiI₆ clusters leads to a collinear antiferromagnetic order at $T_{N1} \simeq 78$ K. Below $T_{N2} \simeq 59.5$ K, NiI₂ enters an imperfect proper-screw helimagnetic phase where ferroelectricity appears simultaneously, induced by inverse Dzyaloshinskii-Moriya interaction [Fig. 1(b)] [1–3]. In this multiferroic phase, the helimagnetic structure has an incommensurate magnetic modulation vector $\mathbf{q} \sim (0.138, 0, 1.457)$. The \mathbf{q} vector has an angle of about 71° with respect to the *ab* plane, and the spin plane has an angle of about 55° with respect to the *c* axis [4]. Hence, the spin plane and the \mathbf{q} vector are not normal to each other. In this sense, NiI₂ has imperfect proper-screw magnetic ordering with broken inversion symmetry [Fig. 1(c)]. The ensuing electric polarization \mathbf{P} lies in the *ab* plane and can be aligned perpendicular to the applied in-plane magnetic field during field cooling [3–6].

Recently, a magnetic exciton mode of Zhang-Rice entangled character and an accompanying two-magnon sideband were discovered in NiI₂ [7,8]. The two-magnon sideband associated with the exciton resonance in NiI₂ implies that low-energy magnon excitations can be found in the terahertz range. Indeed, a previous Raman spectroscopy study reported two excitation modes at 31 and 37.5 cm⁻¹ below T_{N2} in NiI₂, and the possibility of electromagnons was proposed [9,10].

In fact, the presence of multiferroicity in NiI₂ naturally suggests that the low-energy Raman features may indeed be

electromagnons, commonly found in many other multiferroic materials [11–17]. However, these features were not yet reported in neutron scattering experiments, which casts doubt on their existence or their electromagnetic character. Therefore, it is timely to investigate the existence of electromagnons in NiI₂ using other optical measurements, such as terahertz spectroscopy.

In this paper, we report on our terahertz transmission and reflection measurements on NiI₂ single crystals. From our transmission spectra, we observed two electromagnon modes at 34 and 37 cm⁻¹ at 1.5 K below T_{N2} . The polarization, temperature, and magnetic field dependences have been studied in detail. An additional reflection measurement shows that these magnons are indeed electric dipole active rather than magnetic dipole active. Our results show that NiI₂ is an exciting van der Waals platform where an interplay between antiferromagnetism and multiferroicity can be studied via electromagnon excitations.

II. METHOD

Single crystals of NiI₂ were synthesized via the chemical vapor transport method. Ni powder (99.99% Sigma-Aldrich) and crystalline iodine (99.99%, Alfa Aesar) were weighed in the stoichiometric ratio with additional 5% iodine within an argon-filled glove box. The mixture was sealed in a quartz tube, evacuated by a rotary vane pump, and then placed in a two-zone furnace. The temperature was set to reach 750 °C and 720 °C within 6 h. The typical pressure inside the quartz tube was ~1 Pa. The furnace was held in the temperature gradient for 7 days and then cooled slowly to room temperature over 5 days. The grown crystals formed shiny gray flakes, and the typical crystal size was 5 × 5 × 0.1 mm³.

Our terahertz transmission and reflection measurements were performed with a TERA K15 terahertz time-domain spectrometer (Menlo Systems, Germany) coupled with a

*Correspondence author: jgpark10@snu.ac.kr†Correspondence author: super@yonsei.ac.kr

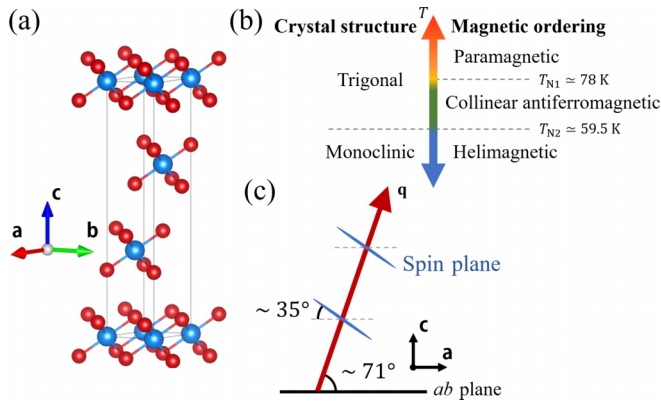


FIG. 1. Crystal structure and magnetic ordering of NiI_2 . (a) Blue spheres indicate Ni atoms and red spheres indicate I atoms. (b) NiI_2 is paramagnetic above $T_{N1} \simeq 78$ K, but it is antiferromagnetic below T_{N1} . Below T_{N2} , NiI_2 additionally acquires multiferroicity. (c) Spin orientation for imperfect proper-screw helimagnetic ordering. Spin plane (blue) is not normal to the \mathbf{q} vector (red).

SpectromagPT magneto-optic cryostat (Oxford Instruments, UK). The SpectromagPT system is a liquid-He-free closed-cycle type and is operated in the temperature range of 1.5–300 K and in the magnetic field range of 0–7 T. The entire terahertz beam path was enclosed in a Plexiglas box purged with nitrogen gas to eliminate water vapor absorption. The NiI_2 crystal sample used for the transmission measurement in Fig. 2(a) had a thickness of 171 μm . The sample was fixed to a gold-coated copper sample holder with Kapton tape. The sample holder had a 3 mm diameter hole. Another NiI_2

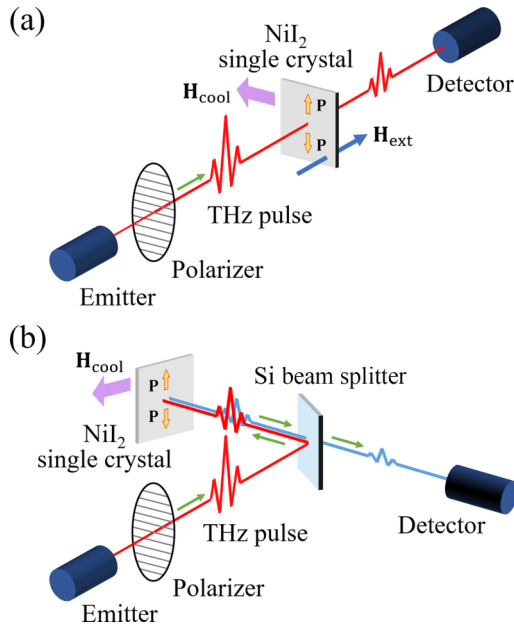


FIG. 2. Schematics of terahertz measurements conducted on NiI_2 : (a) transmission and (b) reflection. \mathbf{H}_{cool} is the in-plane magnetic field applied during the field cooling. \mathbf{P} is the electric polarization formed below $T_{N2} \simeq 59.5$ K during the field cooling. \mathbf{P} is in plane and perpendicular to \mathbf{H}_{cool} . For the transmission experiment (a), an external magnetic field \mathbf{H}_{ext} was applied out of plane.

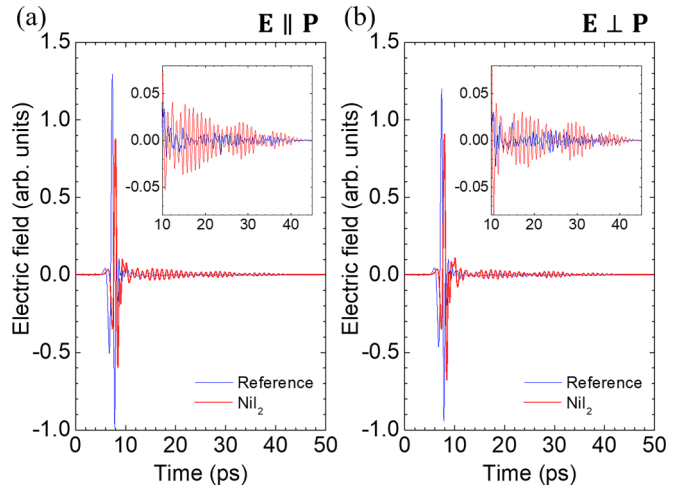


FIG. 3. Terahertz time-domain signals of transmission measurements in (a) $\mathbf{E} \parallel \mathbf{P}$ and (b) $\mathbf{E} \perp \mathbf{P}$ polarizations of terahertz pulse at 1.5 K and $\mathbf{H}_{\text{ext}} = 0$. Blue lines are reference signals, and red lines are the signals of NiI_2 . The inset of each figure shows the long oscillating tail due to absorption peaks.

crystal sample was used for the reflection measurement and had a thickness of 515 μm and a clean, flat surface [Fig. 2(b)]. The sample was fixed to a gold-coated copper sample holder with Kapton tape. The sample holder had a 5 mm diameter hole. A gold-coated mirror was used as the reference, and a single-side polished silicon wafer was used as a beamsplitter.

NiI_2 exhibits a multiferroic phase with imperfect proper-screw helical ordering below T_{N2} . Before terahertz measurements, NiI_2 crystals were cooled under an in-plane magnetic field of 4 T. By this cooling process, an in-plane electric polarization is induced along the direction perpendicular to the cooling magnetic field [3]. We confirmed that its direction was randomly determined in the absence of a cooling field, but that the electric polarization can be reliably and reproducibly formed as long as the cooling field is maintained throughout a thermal cycle. Terahertz spectroscopy measurements, both transmission and reflection, were performed with the polarization of the terahertz pulse electric field \mathbf{E} parallel or perpendicular to the polarization \mathbf{P} oriented by the cooling field \mathbf{H}_{cool} .

III. RESULT AND ANALYSIS

Figure 3 shows terahertz time-domain signals of transmission measurements at $T = 1.5$ K and $\mathbf{H}_{\text{ext}} = 0$. The relaxation of specific excitations produces long oscillating tails in the time-domain signals of the sample. We can Fourier transform a time-domain signal to a spectrum depending on frequency (or energy, wave number). From these spectra, we obtained the transmittance $T(\omega) = |E_{\text{sample}}(\omega)/E_{\text{Hole}}(\omega)|^2$ and calculated the absorbance $A = -\log T$ on frequency domain.

Figure 4 depicts the ab -plane absorbance spectra of NiI_2 obtained by transmission measurements at various temperatures in the absence of an external magnetic field ($\mathbf{H}_{\text{ext}} = 0$). Because the present sample is too thin (171 μm) for us to separate the primary terahertz pulse and the first echo pulse, the spectra contain weak interference fringes due to internal

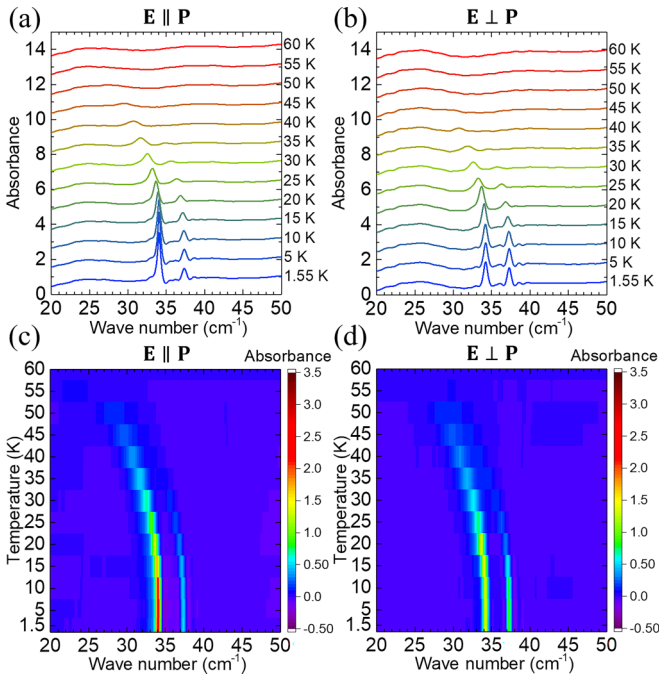


FIG. 4. Temperature and magnetic field dependences of the *ab*-plane absorbance spectra of NiI₂ with (a), (c) $\mathbf{E} \parallel \mathbf{P}$ and (b), (d) $\mathbf{E} \perp \mathbf{P}$ polarizations. (a), (b) Temperature-dependent absorbance spectra of NiI₂ at zero field. (c), (d) The contour plot of the absorbance of NiI₂ at various temperatures relative to the 60 K background.

reflections. Starting from the featureless spectra at 60 K, as NiI₂ enters the multiferroic phase below $T_{N2} \simeq 59.5$ K, two sharp absorption peaks appear, reaching 34 and 37 cm^{-1} at 1.5 K for both $\mathbf{E} \parallel \mathbf{P}$ and $\mathbf{E} \perp \mathbf{P}$ polarizations [Figs. 4(a) and 4(b)]. In order to highlight the temperature dependence, we plotted the difference spectra obtained by subtracting the 60 K spectrum from the raw absorbance spectrum at each temperature [Figs. 4(c) and 4(d)]. We can clearly see that the two absorption peaks weaken and redshift as temperature increases. These absorption signals appear only below the temperature T_{N2} , where NiI₂ exhibits the multiferroic phase, and disappear above T_{N2} . In that sense, we could expect them to be not just thermal excitation modes, but magnetic excitation modes such as magnons. There is substantial anisotropy in the relative intensity between the two magnon modes. In the case of $\mathbf{E} \parallel \mathbf{P}$ polarization, the 34 cm^{-1} peak mode appears very strongly, and the 37 cm^{-1} peak mode appears with a much weaker amplitude. In the case of $\mathbf{E} \perp \mathbf{P}$ polarization, the 34 and 37 cm^{-1} peaks have similar intensities. We check the reproducibility of these intensity ratios by checking that the absorption levels of the two peaks are consistent whenever we had the same field cooling process. It is reported that similar temperature dependence and anisotropy are also observed by Raman spectroscopy [9]. No prominent signals other than these peaks were observed in our terahertz spectra. The energy positions of the magnons are consistent with the previously reported data of the two-magnon sideband in NiI₂ [7].

Under an out of plane external magnetic field \mathbf{H}_{ext} , both absorption modes exhibit magnetic effects. The two peaks

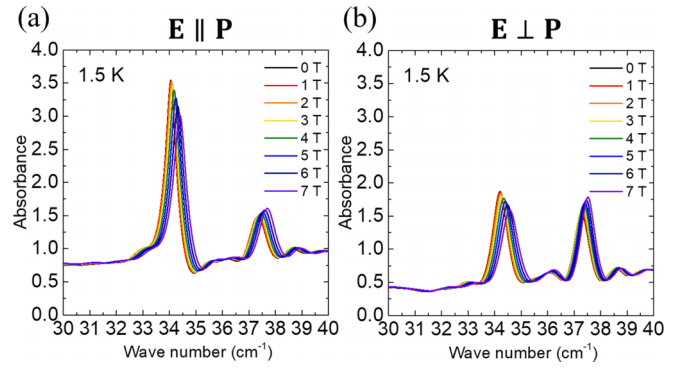


FIG. 5. Out of plane magnetic field dependences of the absorption spectra of NiI₂ at 1.5 K with (a) $\mathbf{E} \parallel \mathbf{P}$ and (b) $\mathbf{E} \perp \mathbf{P}$ polarizations.

blueshift as the field increases from 0 to 7 T at 1.5 K (Fig. 5). In both cases of $\mathbf{E} \parallel \mathbf{P}$ and $\mathbf{E} \perp \mathbf{P}$ polarizations, the 34 cm^{-1} mode weakens and the 37 cm^{-1} mode strengthens as the field increases. The out of plane external magnetic field changes the spin orientation in the helimagnetic ordering, and that leads to a blueshift of the magnetic excitation modes. The magnetic ordering stiffened by external magnetic field becomes difficult to excite. This behavior of magnetic excitation has also been observed in several other multiferroic materials [17–22].

The *ab*-plane reflection measurement was conducted at normal incidence in the energy range of 20 – 50 cm^{-1} [Figs. 6(a) and 6(b)]. Despite the overall similarity among reflectance spectra below T_{N2} , there are prominent “jiggles” in the vicinity of 34 and 37 cm^{-1} . In Figs. 6(c) and 6(d), we highlight these features by the spectra acquired by subtracting the 60 K spectrum as the background from the raw reflectance spectra. These jiggles weaken and redshift as temperature increases, just like the absorption peaks themselves. The signal at 34 cm^{-1} is quite prominent for $\mathbf{E} \parallel \mathbf{P}$ [Fig. 6(c)], although both 34 and 37 cm^{-1} are weak for $\mathbf{E} \perp \mathbf{P}$ [Fig. 6(d)]. With respect to the midpoint resonance position, the jiggle feature shows a local maximum at energies below the center frequency and a local minimum above. This feature then actually indicates that the magnons observed here are electric dipole active. To discuss this, we need to talk about the transmittance and reflectance of single absorption.

The amplitude and phase of a monochromatic electromagnetic wave change when the wave transmits or reflects at the interface of two different media. The change of amplitude is determined by the refractive indices of the two materials, that is, the permittivity and permeability. For a material of permittivity ϵ and permeability μ , the normal-incidence transmission coefficient from material 1 to material 2 is

$$t_{12} = \frac{2\sqrt{\epsilon_1\mu_2}}{\sqrt{\epsilon_1\mu_2} + \sqrt{\epsilon_2\mu_1}}.$$

For convenience, we can set the permittivity and permeability of the free space as unity. Then, the change of monochromatic light of frequency ω including the phase difference is

$$\frac{2\sqrt{\mu}}{\sqrt{\mu} + \sqrt{\epsilon}} e^{i\sqrt{\epsilon\mu}d} \frac{2\sqrt{\epsilon}}{\sqrt{\epsilon} + \sqrt{\mu}} = \frac{4\sqrt{\epsilon\mu}}{(\sqrt{\epsilon} + \sqrt{\mu})^2} e^{i\sqrt{\epsilon\mu}d},$$

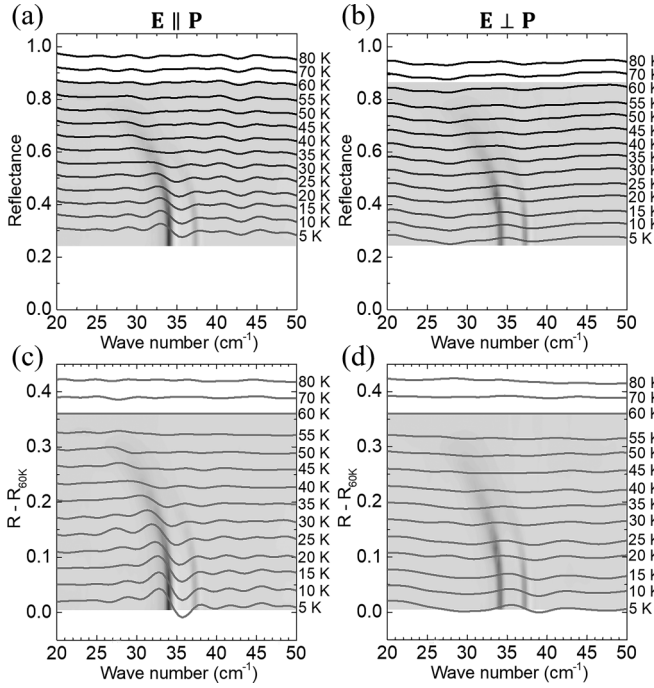


FIG. 6. Temperature-dependent *ab*-plane terahertz reflectance spectra at zero external field ($\mathbf{H}_{\text{ext}} = 0$) for (a), (c) $\mathbf{E} \parallel \mathbf{P}$ and (b), (d) $\mathbf{E} \perp \mathbf{P}$ polarizations. The spectra (a), (b) are of raw reflectance, and the spectra (c), (d) are the raw reflectance minus that at 60 K: $R(T) - R(60 \text{ K})$. The curves were systematically shifted for clarity. The gray background color maps indicate the absorbance displayed in Figs. 4(c) and 4(d).

where d is the thickness of a sample and c is the speed of light. The hole signal for reference passes the free space $\sqrt{\epsilon_0 \mu_0} = 1$ over the distance d , so that the change in the case of hole is just the phase shift, $e^{i\frac{\omega}{c}d}$. Hence, the total transmission coefficient of the sample including the phase difference is

$$t = \frac{4\sqrt{\epsilon\mu}}{(\sqrt{\epsilon} + \sqrt{\mu})^2} e^{i\frac{\omega}{c}(\sqrt{\epsilon\mu}-1)d},$$

which is symmetric with respect to the exchange of ϵ and μ .

On the other hand, the normal-incidence reflection coefficient from material 1 to material 2 is

$$r_{12} = \frac{\sqrt{\epsilon_1 \mu_2} - \sqrt{\epsilon_2 \mu_1}}{\sqrt{\epsilon_1 \mu_2} + \sqrt{\epsilon_2 \mu_1}}.$$

In the special case where material 1 is replaced by free space ($\epsilon_1 = \mu_1 = 1$), the reflection coefficient is simply written by

$$r = \frac{\sqrt{\mu} - \sqrt{\epsilon}}{\sqrt{\mu} + \sqrt{\epsilon}},$$

which is asymmetric with respect to the exchange of ϵ and μ .

Since the transmission coefficient is symmetric with respect to the exchange of ϵ and μ , it is difficult to identify whether a certain absorption is in the electric channel (ϵ) or in the magnetic channel (μ) if we observe the absorption peak by only a transmission measurement. For example, there is the Lorentz oscillator model for describing an absorption in

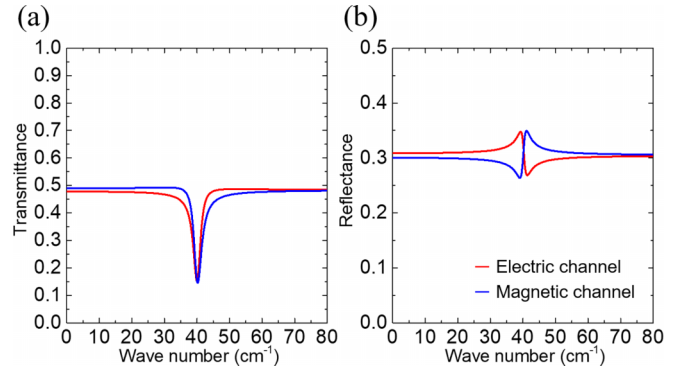


FIG. 7. Simulated (a) transmittance and (b) reflectance spectra due to an absorption peak in the electric and magnetic channels. The red lines are from the electric channel, and the blue lines are from the magnetic channel.

the electric channel,

$$\epsilon(\omega) = \epsilon_\infty + \frac{\omega_p^2}{(\omega_0^2 - \omega^2) - i\omega\gamma}.$$

We simulated a single absorption peak using this Lorentz model. Assuming that it is in the electric channel, the permeability μ is set to unity. Then, we can calculate the transmission spectrum with the Lorentzian permittivity of [$\epsilon_\infty = 12$, $\omega_p = 20 \text{ cm}^{-1}$, $\gamma = 2 \text{ cm}^{-1}$, $\omega_0 = 40 \text{ cm}^{-1}$], shown in Fig. 7(a). The thickness of the sample was set to $d = 200 \mu\text{m}$, as in a typical sample. We can also simulate an absorption peak in the magnetic channel, with a Lorentzian permeability and a constant permittivity. As in the case of permittivity, the transmittance spectrum $T = |t|^2$ for the Lorentzian permeability of [$\mu_\infty = 1$, $\omega_p = 6 \text{ cm}^{-1}$, $\gamma = 2 \text{ cm}^{-1}$, $\omega_0 = 40 \text{ cm}^{-1}$] and a constant permittivity $\epsilon = 12$ is shown in Fig. 7(a). Hence, from a transmission spectrum of a single ordinary absorption peak, we cannot definitely distinguish whether it is from an electric channel (varying ϵ , constant μ) or from a magnetic channel (constant ϵ , varying μ). On the other hand, for each channel given above, the reflection spectra give highly contrasting results. Reflectance, the absolute square of the reflection coefficient spectrum $R = |r|^2$ of each channel, is shown in Fig. 7(b). The spectrum due to the electric channel has an up-down shape, and that from the magnetic channel has a down-up shape. Therefore, the reflectance spectrum can be effectively used to identify the origin of an absorption peak.

Electromagnons are not allowed in the proper-screw-type magnetic ordering by symmetry. However, NiI_2 deviates from perfect proper-screw-type magnetic ordering. The breaking of inversion symmetry then allows for observation of electromagnons [21–23].

Through these analytic discussions, we can identify whether the magnon modes are from an electric channel or from a magnetic channel. Comparison with our experimental results shows that the observed magnon modes are electric dipole active, because the reflectance spectra have an up-down shape.

IV. CONCLUSION

By performing terahertz transmission and reflection measurements, we observed two electromagnon excitation modes at 34 and 37 cm^{-1} in single-crystal NiI_2 and studied their temperature and magnetic field dependences. From the reflectance spectra, which are bound to be asymmetric about the difference between permittivity ϵ and permeability μ , we confirmed that the two modes observed are electromagnons, the magnetic quantum excitations excited by an electric field. Our study shows that the combination of transmission and reflection spectra studies is an effective method to eluci-

date the nature of electromagnetic excitation in multiferroic van der Waals materials.

ACKNOWLEDGMENTS

The work at CQM and SNU was supported by the Leading Researcher Program of the National Research Foundation of Korea (Grant No. 2020R1A3B2079375). The work at Yonsei University was supported by National Research Foundation (NRF) grants funded by the Korean government (MSIT, Grant No. 2021R1A2C3004989), and the SRC program (vdWMRC, Grant No. 2017R1A5A1014862).

-
- [1] H. Katsura, N. Nagaosa, and A. V. Balatsky, Spin Current and Magnetoelectric Effect in Noncollinear Magnets, *Phys. Rev. Lett.* **95**, 057205 (2005).
- [2] T. Kurumaji, Spiral spin structures and skyrmions in multiferroics, *Phys. Sci. Rev.* **5**, 20190016 (2020).
- [3] T. Kurumaji, S. Seki, S. Ishiwata, H. Murakawa, Y. Kaneko, and Y. Tokura, Magnetoelectric responses induced by domain rearrangement and spin structural change in triangular-lattice helimagnets NiI_2 and CoI_2 , *Phys. Rev. B* **87**, 014429 (2013).
- [4] S. R. Kuindersma, J. P. Sanchez, and C. Haas, Magnetic and structural investigations on NiI_2 and CoI_2 , *Physica B+C (Amsterdam)* **111**, 231 (1981).
- [5] M. A. McGuire, Crystal and magnetic structures in layered transition metal dihalides and trihalides *Crystals* **7**, 121 (2017).
- [6] J. M. Friedt, J. P. Sanchez, and G. K. Shenoy, Electronic and magnetic properties of metal diiodides MI_2 ($M = \text{V}, \text{Cr}, \text{Mn}, \text{Fe}, \text{Co}, \text{Ni}, \text{and Cd}$) from 129I Mössbauer spectroscopy, *J. Chem. Phys.* **65**, 5093 (1976).
- [7] S. Son, Y. Lee, J. H. Kim, B. H. Kim, C. Kim, W. Na, H. Ju, S. Park, A. Nag, K.-J. Zhou, Y.-W. Son, H. Kim, W.-S. Noh, J.-H. Park, J. S. Lee, H. Cheong, J. H. Kim, and J.-G. Park, Multiferroic-enabled magnetic-excitons in 2D quantum-entangled van der Waals antiferromagnet NiI_2 , *Adv. Mater.* **34**, 2109144 (2022).
- [8] S. R. Kuindersma, P. R. Boudewijn, and C. Haas, Near-infrared $d-d$ transitions of NiI_2 , $\text{CdI}_2:\text{Ni}^{2+}$, and CoI_2 , *Phys. Status Solidi* **108**, 187 (1981).
- [9] Q. Song, C. A. Occhialini, E. Ergeçen, B. Ilyas, D. Amoroso, P. Barone, J. Kapeghian, K. Watanabe, T. Taniguchi, A. S. Botana, S. Picozzi, N. Gedik and R. Comin, Evidence for a single-layer van der Waals multiferroic, *Nature (London)* **602**, 601 (2022).
- [10] H. Liu, X. Wang, J. Wu, Y. Chen, J. Wan, R. Wen, J. Yang, Y. Liu, Z. Song, and L. Xie, Vapor deposition of magnetic vdW NiI_2 crystals, *ACS Nano* **14**, 10544 (2020).
- [11] M. Cazayous, Y. Gallais, A. Sacuto, R. de Sousa, D. Lebeugle, and D. Colson, Possible Observation of Cycloidal Electromagnons in BiFeO_3 , *Phys. Rev. Lett.* **101**, 037601 (2008).
- [12] W. Azeem, S. Riaz, A. Bukhtiar, S. Sajjad Hussain, Y. Xu, and S. Naseem, Ferromagnetic ordering and electromagnons in microwave synthesized BiFeO_3 thin films, *J. Magn. Magn. Mater.* **475**, 60 (2019).
- [13] S. Pailhès, X. Fabrèges, L. P. Régnault, L. Pinsard-Godart, I. Mirebeau, F. Moussa, M. Hennion, and S. Petit, Hybrid Goldstone modes in multiferroic YMnO_3 studied by polarized inelastic neutron scattering, *Phys. Rev. B* **79**, 134409 (2009).
- [14] A. Pimenov, A. Shuvaev, A. Loidl, F. Schrettle, A. A. Mukhin, V. D. Travkin, V. Yu. Ivanov, and A. M. Balbashov, Magnetic and Magnetoelectric Excitations in TbMnO_3 , *Phys. Rev. Lett.* **102**, 107203 (2009).
- [15] A. B. Sushkov, R. Valdés Aguilar, S. Park, S.-W. Cheong, and H. D. Drew, Electromagnons in Multiferroic YMn_2O_5 and TbMn_2O_5 , *Phys. Rev. Lett.* **98**, 027202 (2007).
- [16] P. Rovillain, J. Liu, M. Cazayous, Y. Gallais, M.-A. Measson, H. Sakata, and A. Sacuto, Electromagnon and phonon excitations in multiferroic TbMnO_3 , *Phys. Rev. B* **86**, 014437 (2012).
- [17] A. Pimenov, A. M. Shuvaev, A. A. Mukhin, and A. Loidl, Electromagnons in multiferroic manganites, *J. Phys.: Condens. Matter* **20**, 434209 (2008).
- [18] Y. Takahashi, R. Shimano, Y. Kaneko *et al.*, Magnetoelectric resonance with electromagnons in a perovskite helimagnet, *Nat. Phys.* **8**, 121 (2012).
- [19] S. Kibayashi, Y. Takahashi, S. Seki *et al.*, Magnetochiral dichroism resonant with electromagnons in a helimagnet, *Nat. Commun.* **5**, 4583 (2014).
- [20] S. Bordács, V. Kocsis, Y. Tokunaga, U. Nagel, T. Rõm, Y. Takahashi, Y. Taguchi, and Y. Tokura, Unidirectional terahertz light absorption in the pyroelectric ferrimagnet $\text{CaBaCo}_4\text{O}_7$, *Phys. Rev. B* **92**, 214441 (2015).
- [21] N. Kida, S. Kumakura, S. Ishiwata, Y. Taguchi, and Y. Tokura, Gigantic terahertz magnetochromism via electromagnons in the hexaferrite magnet $\text{Ba}_2\text{Mg}_2\text{Fe}_{12}\text{O}_{22}$, *Phys. Rev. B* **83**, 064422 (2011).
- [22] N. Kida and Y. Tokura, Terahertz magnetoelectric response via electromagnons in magnetic oxides, *J. Magn. Magn. Mater.* **324**, 3512 (2012).
- [23] J. Vít, F. Kadlec, C. Kadlec, F. Borodavka, Y. S. Chai, K. Zhai, Y. Sun, and S. Kamba, Electromagnon in the Y-type hexaferrite $\text{BaSrCoZnFe}_{11}\text{AlO}_{22}$, *Phys. Rev. B* **97**, 134406 (2018).